A theoretical and experimental evaluation of III–nitride solar-blind UV photocathode*

Bin Ren(任彬)[1,2,3,†], Hui Guo(郭晖)[1,3], Feng Shi(石峰)[1,3], Hong-Chang Cheng(程宏昌)[1,3], Hui Liu(刘晖)[1,3], Jian Liu(刘健)[4], Zhi-Hui Shen(申志辉)[5], Yan-Li Shi(史衍丽)[3], and Pei Liu(刘培)[6]

[1] *Science and Technology on Low-Light-Level Night Vision Laboratory, Xi'an* 710065, *China*
[2] *Department of Physics, Beijing Institute of Technology, Beijing* 100081, *China*
[3] *Kunming Institute of Physics, Kunming* 650223, *China*
[4] *Institute of Electron Engineering and Photoelectric Technology, Nanjing University of Science and Technology, Nanjing* 210094, *China*
[5] *Chongqing Optoelectronics Research Institute, Chongqing* 400060, *China*
[6] *Newcastle University Business School, Newcastle, The UK*

(Received 10 February 2017; revised manuscript received 14 April 2017; published online 20 June 2017)

We have developed a superior solar-blind ultraviolet (UV) photocathode with an $Al_xGa_{1-x}N$ photocathode ($x \sim 0.45$) in semi-transparent mode, and assessed spectra radiant sensitivity related to practical use. Before being grown over a basal plane sapphire substrate by low-pressure metal organic chemical vapor deposition (MOCVD), a reasonable design was made to the photocathode epitaxy structure, focusing on the $Al_xGa_{1-x}N$: Mg active layer, then followed by a comprehensive analysis of the structural and optical characterization. The spectra radiant sensitivity is peaked of 41.395 mA/W at wavelength 257 nm and then decreases by about 3 to 4 decades at 400 nm demonstrating the ability of this photocathode for solar-blind application prospects.

Keywords: photocathode, III–nitride, solar-blind UV

PACS: 85.60.Ha, 73.61.Ey, 79.60.–I

DOI: 10.1088/1674-1056/26/8/088504

1. Introduction

Many ultraviolet (UV) detection scenarios of military and civil applications, such as missile approaching warning systems and astronomy applications, require an extremely high sensitivity to UV radiation relative to any signal at lower energy.[1–3] Recently the development of AlGaN materials for UV detectors are becoming popular and attracting intense research. As a direct-band-gap material, $Al_xGa_{1-x}N$ compounds can be tailored for the optimized detection long wavelength cut off in the UV spectrum, which offers the most viable approach toward the realization of high efficiency UV photon detectors, especially in airborne and space applications which require the most lightweight and simple device possible.

Photocathode-based image intensifiers always have the advantage over solid state devices in this acknowledgement as the dark current is inherently low.[4–7] Many research groups have performed experimental studies to discuss the GaN or low aluminum mole component AlGaN photocathodes for the visible-blind UV image intensifier tube.[8–12] In this work, we have developed a photocathode that combined two III–nitride epilayers with different alloy compositions, and identified it to be a true solar-blind UV photocathode with the threshold wavelength to be cutoff as 280 nm.

2. Structure and detection mechanism

We proposed a prototype of semi-transparent type III–nitrides photocathode as shown in Fig. 1. The incident light passes through the quartz glass plate, antireflect layer MgF_2, and sapphire substrate, then reaches the AlN layer. The buffer layer AlN functions as a window layer of the photocathode and determines the short-wavelength threshold of the spectral response, which is at about 200 nm (corresponding to AlN's energy band gap of 6.2 eV). The light is absorbed and generates photoelectrons in the AlGaN-active layer, then they diffuse to the surface, and emit into a vacuum.[13,14]

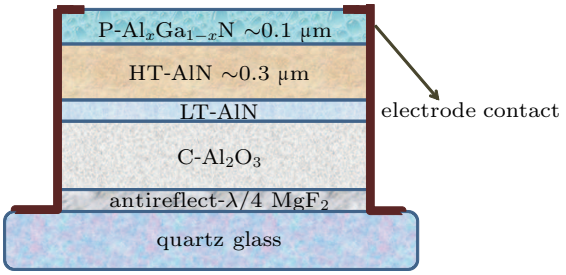


Fig. 1. (color online) Schematic cross section of AlN/AlGaN photocathode.

Thin film was chosen to allow efficient emission of photoelectrons generated at the back of the film for operation in the semi-transparent mode. The optical absorption rises with the

*Project supported by the National Natural Science Foundation of China (Grant No. 10974015) and the National Defense Pre-Research Foundation of China (Grant No. 9140C380502150C38002).

†Corresponding author. E-mail: robinson_cv@163.com

© 2017 Chinese Physical Society and IOP Publishing Ltd

increasing of the AlGaN thickness. Thicker films would result in lower emission efficiency because of higher probability of recombination or trapping of the photo-generated electrons before diffusing to the vacuum surface. While thinner films would lower the quantum efficiency by reducing the absorption of the incident photons. Therefore, the trade-off within both factors determines the optimum thickness of the AlGaN active layer. According to the first-order approach model, it is reasonable to assume that the optimum thickness of the active layer can be expressed by formula (1) on an AlGaN semi-transparent-type solar-blind UV photocathode.[15,16]

$$T = \frac{\ln(\alpha L)}{\alpha - (1/L)}, \tag{1}$$

where, the absorption coefficient α is assumed to obey the following expression of formula (2a). Optical band gap E_g varies as a quadratic function of Al mole fraction where the bowing parameter equals to 1.08 for $Al_xGa_{1-x}N$ at room temperature. Expressing E_g and $h\upsilon$ in electrovolts unit we receive the absorption coefficient in μm^{-1}. L is the minor carrier attenuation length in the range of 0.02 μm∼ 0.2 μm on a reasonable assumption according to Ref. [17].

$$\alpha = 2.3 \times 10^5 (h\upsilon - E_g)^{1/2}, \tag{2a}$$

$$E_g = 6.13x + 3.42(1-x) - 1.08x(1-x). \tag{2b}$$

The threshold wavelength of 280 nm was realized by controlling the Al mole fraction to equal 0.45. In addition, the theoretical basis for this structure is that the AlN/AlGaN heterosturcture sub-surface layer has a wider band-gap than the AlGaN top layer. Then, in principle, photo-electrons that are excited into the conduction band, but away from the surface would meet the higher band gap of the sub-surface AlN buffer layer, and they are reflected back toward the vacuum surface. This of course could increase the efficiency of the photocathode. We assume a linear relationship of electron affinity AFF in the III–nitride system: $\mathrm{AFF} = 4.1 - Ax$, where x represents the Al mole-fraction as before, $A = 1.44$ eV or 2.30 eV, corresponding to the extremes of the band-offset values quoted by Ambacher.[18] Thus, the conduction band discontinuities between $Al_{0.45}Ga_{0.55}N$ and AlN lie in the range of $\Delta E_c \in [0.63, 1.04]$ eV. A Mg-heavily doping level as high as 1×10^{19} cm^{-3} is required to facilitate the forming of effective negative electron affinity (NEA).[19]

3. Experiment and discussion

The samples used in this study were grown by low-pressure MOCVD in an Aixtron 200/4 HT horizontal flow reactor. Tri-methyl gallium (TMGa), tri-methyl aluminum (TMAl), and ammonia (NH3) were used as the precursors and bis-cyclopentadienyl magnesium (Cp2Mg) was used as the precursor for the Mg doping. These precursors were introduced into the reactor with purified hydrogen as the carrier gas.[20] The substrate of basal plane (001) sapphire was double-side-polished to allow for the realization of semi-transparent photocathode. Prior to the growth, the sapphire substrates were thermal cleaned in hydrogen ambient at 1100 °C, similar to that of other researchers.[21] A low-temperature nucleation layer AlN was first grown on 2 inch-diameter (1 inch = 2.54 cm), 0.4-mm thick (0001) *c*-sapphire substrates at 850 °C, followed by 0.3-μm high-temperature buffer layer AlN at 1200 °C, indicated as the window layer, and 0.1-μm $Al_{0.45}Ga_{0.55}N$ at 1150 °C was grown, indicated as the active layer. The typical pressure was 50 mbar (1 bar = 10^5 Pa), the V/III ratio during growth of the Mg-doped $Al_{0.45}Ga_{0.55}N$ layer was varied by varying the NH_3 flow rate. Post-growth, the p-type conductivity was enhanced using a 10-min 750-°C N_2 ambient anneal to activate the Mg acceptors.

3.1. Structural characterization

Structural information was obtained using a PANalytical X' Pert MRD high-resolution (0.0001°) x-ray diffractometer (HRXRD) with a front Bartels-type monochromator [4 × Ge (220)]. Characteristic x rays ($\lambda = 1.540598$ Å) of Cu $K_{\alpha 1}$ were used to probe samples. Both ω–2θ rocking curves, scans around the symmetric (0002) plane, and reciprocal space mapping (RSM), scans around the asymmetric $(10\bar{1}4)$ plane, using a triple-axis detector were obtained, as shown in Fig. 2 and Fig. 3. RSM was used to estimate the strain and relaxation between AlGaN and AlN layer. From Fig. 2, two discrete peaks on maps of III–nitride films were clearly observed, the AlGaN film reciprocal lattice point (RLP) did not fall exactly on the vertical line that is perpendicular to the q_x axis and includes the RLP of AlN buffer. This indicates that AlGaN is not fully strained but approaching 100% relaxation with respect to the underlying AlN material. The characteristics of AlGaN were evaluated from (0002) ω–2θ scan by HRXRD from Fig. 3, the main strong peaks are the (0002) zeroth-order Bragg reflection of thick AlN buffer layer, the weak and

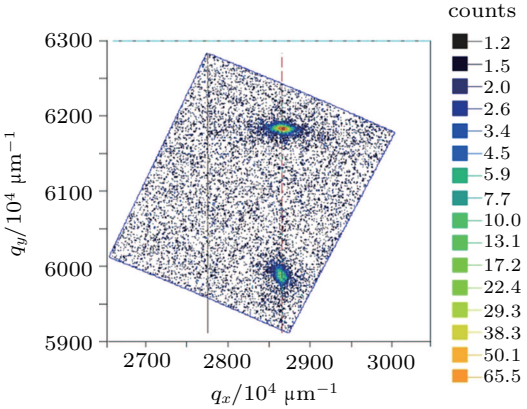


Fig. 2. (color online) Experimental RSM close to the symmetrical $(10\bar{1}4)$ AlGaN reflection for the irradiated sample.

broad peaks at the left side of the main peaks correspond to the (0002) zeroth-order Bragg reflection of thin AlGaN active layers. The composition and thickness of the AlGaN epitaxial layers were determined from the simulation of the XRD data using the X' Pert epitaxy software based on simple kinematical theory.[22] The fitting approach usually followed by two steps, firstly, to simulate experimental data by convoluting broadened models together, such as instrument parameters as well as sample parameters; secondly, followed by fitting the model to the experimental data.[23,24] The thickness values of active layer obtained from X' Pert epitaxy software corroborate with the *in situ* monitored reflectometric patterns of the MOCVD and are in accordance with the design values shown in Fig. 1. PendellÖsung fringes in Fig. 3 clearly further indicate that the heterostructure interface is smooth and the thickness and alloy composition are well controlled, with high quality of the epitaxy layers.

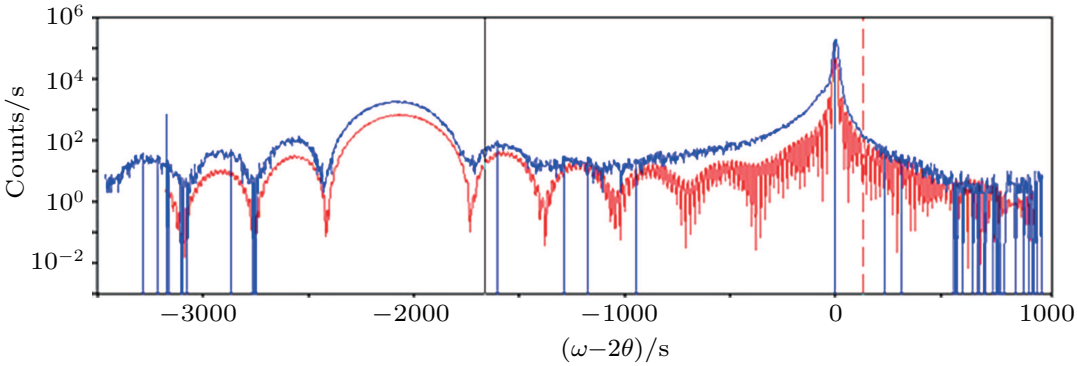


Fig. 3. (color online) The (0002) ω–2θ scan curves of the irradiated sample, obtained using an analyser crystal.

3.2. Optical characterization

The transmission spectra of the sample measured at room temperature are shown in Fig. 4. We can observe that the transmittance vary significantly with the wavelength of 280 nm, and the average transmittance below the energy band of the spectra was highter than 70%. The sharp cutoff and well-defined fringes of the transmittance spectrum for the sapphire/AlN/AlGaN epitaxy layer confirmed the high-quality of the material and smooth interface.

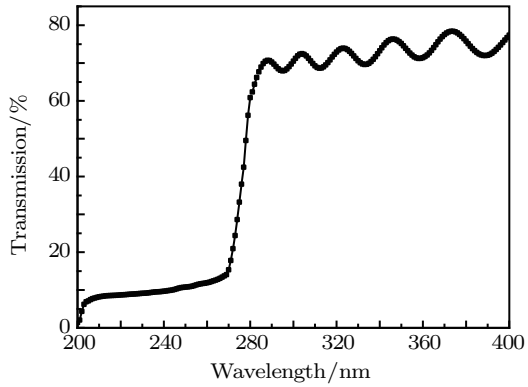


Fig. 4. Transmittance spectrum of sapphire/AlN/AlGaN heterostructure photocathode.

3.3. Spectra radiant sensitivity

The AlGaN photocathode was prepared as shown in Fig. 5(a) corresponding to Fig. 1. Then, the AlGaN-based photocathode was enveloped with MCP and phosphor to a proximity-focused image intensifier tube, as shown in Fig. 5(b). The spectra radiant sensitivity of an AlGaN photocathode was measured using a UV spectrometer as follows in Fig. 6. A deuterium lamp filtered by a monochromator was used as the light sources for the UV region. The UV light that emerged from the spectrometer was coupled into one end of a UV-enhanced fiber. The other end of the fiber was precisely collimated over the device under test. The incident power was monitored by a standard calibrated Si photodiode as the identical illumination conditions.[25]

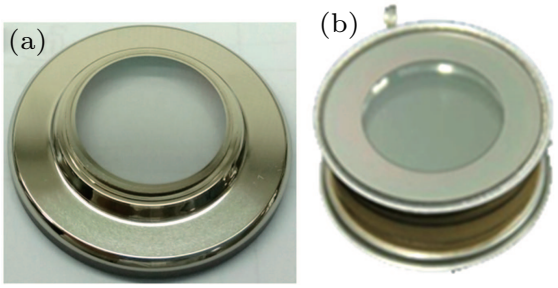


Fig. 5. (color online) $Al_xGa_{1-x}N$ photocathode (a) and solar-blind image intensifier tube (b).

The radiant sensitivity was calculated from the ratio of the photoemission current to the reference Si photodiode current. Figure 7 shows the spectral responsivity for this photocathode, the responsivity between 220 nm to 280 nm was relatively flat and with small fluctuation depending on wavelength. The responsivity is peaked of 41.390 mA/W at wavelength 257 nm and then decreased by about 3 to 4 decades at 400 nm. In particular the spectral response exhibited a sharp cutoff at the AlGaN band gap energy corresponding to 280 nm, and remained at low response for the entire near UV spectrum, thus demonstrating the ability of the intensifier tube for solar-blind applications.[26]

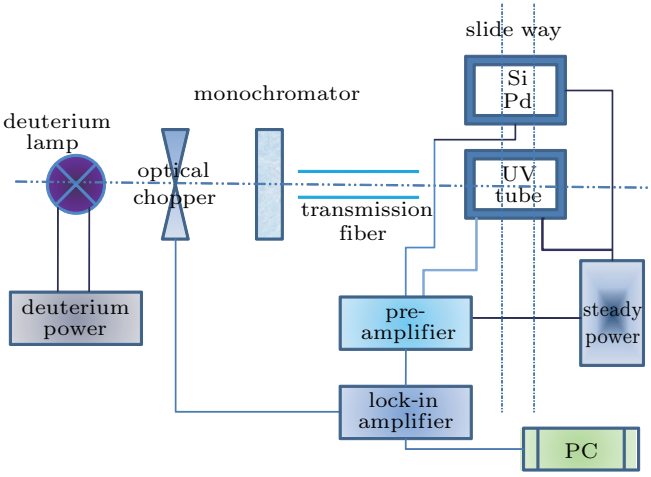


Fig. 6. (color online) Spectral responsivity measurement schematics for $Al_xGa_{1-x}N$ solar-blind image intensifier.

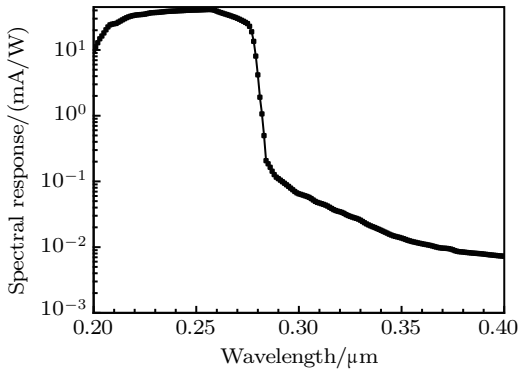


Fig. 7. Spectral responsivity of the $Al_xGa_{1-x}N$ photocathodes image intensifier with $x = 0.45$.

4. Conclusion and perspectives

In this paper, we have developed an AlGaN photocathode which can eliminate the need for external filtering to achieve true solarblind operation, and the important physical effects that will influence photocathode performance have also been analyzed. From the simulation result of high resolution x-ray diffraction (HRXRD) ω–2θ curve by using kinetic diffraction theory, the Al composition in the active layer was determined to be about 45%, and the UV spectral meter also verified this. We obtained a relative flat and high quantum efficiency from a wavelength between 220 nm to 280 nm and fell sharply by three to four orders of magnitude for wavelengths above 280 nm, and the peak responsivity reached up to 41.395 mA/W at 257 nm. We believe that the photocathode reported in this article represents an advancement toward achieving high-quality solar-blind UV photodetectors.

References

[1] Sun J D, Qin H, Lewis R A, Sun Y F, Zhang X Y, Cai Y, Wu D M and Zhang B S 2012 *Appl. Phys. Lett.* **100** 173513
[2] Wang H, Jin X L, Chen C P, Tian M F and Zhu K H 2015 *Chin. Phys. B* **24** 038501
[3] Hu Z F, Wu H H, Lv Y W and Zhang X Q 2015 *Chin. Phys. B* **24** 107302
[4] Ulmer M P, Wessels B W and Siegmund O H W 2003 *Proc. SPIE* **4854** 225
[5] Jiao G C, Liu Z T, Guo H and Zhang Y J 2016 *Chin. Phys. B* **25** 048505
[6] Lee C J, Kwon Y J, Won C H, Lee J H and Hahm S H 2013 *Appl. Phys. Lett.* **103** 111110
[7] Malinowski P E, Duboz J Y, Moor P D, Minoglou K, John J, Horcajo S M, Semond F, Frayssinet E, Verhoeve P, Esposito M, Giodanengo B, BenMoussa A, Mertens R and Hoof C V 2014 *Appl. Phys. Lett.* **98** 141104
[8] Liu Z, Machuca F, Pianetta P, Spicer W E. and Pease R F 2004 *Appl. Phys. Lett.* **85** 1541
[9] Yang Y F, Fu R G, Zhang Y J, Wang X H and Zou J J 2012 *Acta Phys. Sin.* **61** 068501 (in Chinese)
[10] Fu X Q, Chang B K, Qian Y S and Zhang J J 2012 *Chin. Phys. B* **21** 030601
[11] Wang X H, Chang B K, Ren L and Gao P 2011 *Appl. Phys. Lett.* **98** 082109
[12] Fu X Q, Chang B K, Wang X H, Li B, Du Y J and Zhang J J 2011 *Chin. Phys. B* **20** 037902
[13] Zhang Y J, Zou J J, Wang X H, Chang B K, Qian Y S, Zhang J J and Gao P 2011 *Chin. Phys. B* **20** 048501
[14] Fu X Q, Chang B K, Qian Y S and Zhang J J 2012 *Chin. Phys. B* **21** 030601
[15] Jia X Z 2013 *Negative Electron Affinity Photocathodes and Applications* (Beijing: National Defense Industry Press) p. 122
[16] Wang X H, Shi F, G H, Hu C L, Cheng H C, Chang B K, Ren L, Du Y J and Zhang J J 2012 *Chin. Phys. B* **21** 087901
[17] Siegmund O, Vallerga J, Mcphate J, Malloy J, Tremsin A, Martin A, Ulmer M and Wessels B 2006 *Nucl. Instrum. Methods Phys. Res. A* **567** 89
[18] Ambacher O 1998 *J. Phys, D: Appl. Phys.* **31** 2653
[19] Grabowski S P, Schneider M, Nienhaus H, Monch W, Dimitrov R, Ambacher O and Stutzmann M 2001 *Appl. Phys. Lett.* **78** 2503
[20] Leopold D J, Buckley J H and Rebillot P 2005 *J. Appl. Phys.* **98** 043525
[21] Cicek E, Vashaei Z, Clintock R M and Razeghi M 2011 *Proc. SPIE* **8155** 8155O
[22] He Y, Sun Y T, Zhao Y M, Yu S Z and Dong J T 2017 *Chin. Phys. B* **26** 038102
[23] Asif F, Lachab M, Coleman A, Ahmad I, Zhang B, Adivarahan V and Khan A 2014 *JVSTB* **32** 061204
[24] Sanjay Kr, Jana, Saptarsi Ghosh, Syed Mukulika Dinara, Mihir Mahata, Soumen Das and Dhrubes Biswas 2015 *JVSTB* **33** 041206
[25] Yang Y F, Fu R G, Ma L, Wang X H and Zhang Y J 2012 *Acta Phys. Sin.* **61** 128504 (in Chinese)
[26] Duboz J Y, Grandjean N, Omnes F, Mosca M and Reverchon J L 2005 *Appl. Phys. Lett.* **86** 063511